Optimizing H1 cavities for the generation of entangled photon pairs

Matthieu Larqué, Timothy Karle, Isabelle Robert-Philip, Alexios Beveratos

Optimizing H1 cavities for the generation of entangled photon pairs

M. Larque, T. Karle, I. Robert-Philip and A. Beveratos

Laboratoire de Photonique et Nanostructures LPN-CNRS UPR-20, Route de Nozay, 91460 Marcoussis, France

E-mail: `Alexios.Beveratos@lpn.cnrs.fr`

Abstract. We report on the theoretical investigation of photonic crystal cavities etched on a suspended membrane for the generation of polarization entangled photon pairs using the biexciton cascade in a single quantum dot. The implementation of spontaneous emission enhancement effect increases the entanglement visibility, while the concomitant preferential funneling of the emission in the cavity mode increases the collection of both entangled photons. We demonstrate and quantify that standard cavity designs present a polarization dependent emission diagram, detrimental to entanglement. The optimization of H1 cavities allows to obtain both high collection efficiencies and polarization independent emission, while keeping high Purcell factors necessary for high quality entangled photon sources.

PACS numbers: 42.55.Tv, 03.67.Bg, 03.67.Mn,78.67.Hc

Submitted to: *New J. Phys.*

Entangled photon sources play an important role in quantum communication networks or quantum information processing [1, 2]. For the former, they are a necessary resource for the realization of quantum repeaters [3] based on quantum teleportation or quantum entanglement swapping. In the first demonstrations of such relays, parametric down conversion sources have been used for the generation of entangled photon pairs [4, 5, 6, 7]. Such non-linear sources of entanglement can combine narrow spectral bandwidths with a maximal generation rate [7, 8, 9]. Although these sources may be very useful and easy to implement, they always suffer from the Poissonian statistics of the emitted photons pairs leading to multipair emission and thus decreasing the fidelity of entanglement [10]. Being able to produce polarization entangled photon pairs on demand would be an important step towards robust quantum relays. Such sources can be obtained from the biexciton-exciton cascade emission of a single quantum dot [11], and first experimental demonstrations have been reported [12, 13]. Obtaining entangled photons pairs, however, from such quantum dots sources with both high fidelity and high collection efficiency remains a problem. Implementing Cavity Quantum ElectroDynamics effects by embedding a single quantum dot in a microcavity could not only improve the fidelity of the emitted pair [14] by taking advantage of the Purcell effect, but also by enhance the collection efficiency [15, 16]. One promising microcavity for such purpose is the single defect hole cavity in a triangular lattice of holes (H1) etched on a suspended membrane, due to its small mode volume and its polarization degeneracy. However, in a standard H1 cavity, the radiation pattern of the two fundamental degenerate modes do not overlap, leading to photon distinguishability and thus destroying entanglement. Theoretical calculations demonstrate that this radiation pattern can be strongly modified by changing, for instance, the position of the holes surrounding the defect [17]. This modification of the design is necessary to avoid distinct emission patterns. This emission pattern distinguishability is related to the mode overlap.

In this paper, we report on the theoretical investigation of H1 photonic crystal cavities etched on slab membrane, in order to obtain both high collection efficiencies for both photons and a high overlap between the two fundamental energy-degenerate modes. The dependency of the Bell inequalities as a function of the mode overlap is derived. We also investigate the impact of the position of the quantum dot inside the cavity on entanglement visibility and collection efficiency.

1. Entangled state density matrix for non overlapping modes

Polarization entangled photon pairs can only be obtained if and only if, even in principle, the polarization of the photon can not be determined by measuring another degree of freedom as for example the photon's energy. In the same way, if the emission mode of one of the photons of the pair does not perfectly match the emission mode of the other photon, the non-maximal overlap between the two emission modes will reduce the fidelity of entanglement. Our analytical derivation of this non-maximal mode overlap

effect is based on the density matrix of the photon pair emitted by the cascade emission from the biexcitonic level of a single quantum dot.

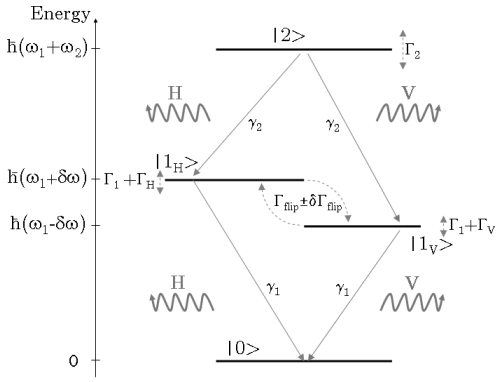

Figure 1. Schematic description of the two-photon cascade in a typical quantum dot four-level system with an energy splitting $2\hbar\delta\omega$ of the relay level, yielding two collinearly polarized photons (either H or V).

The eigenbasis of the dot involves four levels : $|2\rangle$ (biexcitonic level), $|1_H\rangle$ and $|1_V\rangle$ (two excitonic levels with opposite angular momenta) and $|0\rangle$ (fundamental level). In this eigenbasis, the emitted photons are linearly polarised along the horizontal (H) or vertical (V) directions. The density matrix of the photon pair in this particular basis $\mathcal{B} = [H_1H_2, H_1V_2, V_1H_2, V_1V_2]$ where the subscript $i = 1, 2$ is related to the photon emitted by the biexcitonic level and excitonic level respectively, can be written in the form [14]:

$$\overline{\rho} = \begin{pmatrix} \alpha & 0 & 0 & d - ic_1 \\ 0 & \frac{1}{2} - \alpha & c_2 & 0 \\ 0 & c_2 & \frac{1}{2} - \alpha & 0 \\ d + ic_1 & 0 & 0 & \alpha \end{pmatrix} \tag{1}$$

where:

$$\begin{aligned} \alpha &= \frac{1}{2}\frac{\gamma_1 + \Gamma_{flip}}{\gamma_1 + 2\Gamma_{flip}} \\ d &= \frac{1}{2}\frac{\gamma_1(\gamma_1 + 2\Gamma + \Gamma_{flip})}{(2\delta\omega)^2 + (\gamma_1 + \Gamma_{flip} + \Gamma)^2 - (\delta\Gamma_{flip})^2} \\ c_1 &= \frac{1}{2}\frac{\gamma_1\delta\omega}{(2\delta\omega)^2 + (\gamma_1 + \Gamma_{flip} + \Gamma)^2 - (\delta\Gamma_{flip})^2} \\ c_2 &= \frac{1}{2}\frac{\gamma_1\delta\Gamma_{flip}}{(2\delta\omega)^2 + (\gamma_1 + \Gamma_{flip} + \Gamma)^2 - (\delta\Gamma_{flip})^2} \end{aligned} \tag{2}$$

with γ_1 the exciton decay rate. $\Gamma = \Gamma_H + \Gamma_V$ is the cross-dephasing rate between the two excitonic states. $\Gamma_{flip} \pm \delta\Gamma_{flip}$ describe phenomenologically relaxation mechanisms between the two excitation states, leading to incoherent population transfers between these two states ($\delta\Gamma_{flip}$ takes into account the possible rate asymmetry in this process). $\delta\omega$ is the energy splitting of the excitonic levels. Γ_1 is the pure dephasing rate induced by

dephasing processes that occur simultaneously and attach the same information to the phase and energy of these two excitonic levels. Γ_H and Γ_V are polarization-dependent pure dephasing rates induced by dephasing processes that do not identically affect the two relay levels and whose impact depends on the polarization of the excitonic states.

We consider that the exciton and biexciton photons are emitted in the same cavity mode, ie the cavity mode is resonant with both transitions. The cavity mode is doubly-degenerate in polarisation, due to the C_6 symmetry of the H1 cavity. We can consequently describe the photons polarization in the (H, V) basis defined previously, independently of the orientation of the dot with regards to the orientation of the photonic crystal. We define $\Phi_H(\vec{r})$ (resp. $\Phi_V(\vec{r})$) the complex spatial far field distribution of the horizontal (H) (resp. vertical (V)) polarization modes. Propagation occurs along the orthogonal direction to the photonic crystal membrane and $\vec{r}$ denotes the radial vector perpendicular to the propagation axis. The density matrix can be rewritten under the form:

$$\rho(\vec{r_1},\vec{r_2})_{xy,uv} = \Phi_x(\vec{r_1})^\dagger * \Phi_y(\vec{r_2})^\dagger * \overline{\rho}_{xy,uv} * \Phi_u(\vec{r_1}) * \Phi_v(\vec{r_2}) \tag{3}$$

with xy and $uv \in \mathcal{B}$ and $\overline{\rho}_{xy,uv}$ being the density matrix element on line xy and column uv. $\rho(\vec{r_1},\vec{r_2})_{xy,uv}$ is the density matrix element on line xy and column uv of the new density matrix $\rho(\vec{r_1},\vec{r_2})$. Let $t(r)$ be the function describing the detectors' active areas which are placed along the propagation axis. There are in fact two distinctive detectors (one for each photon of the pair [14]) but we suppose that they have the same sensitive area for the sake of simplicity. The density matrix can be reduced for the detected photon pairs to:

$$\rho = \frac{\int d^2r_1\ d^2r_2\ t(\vec{r_1})t(\vec{r_2})\rho(\vec{r_1},\vec{r_2})}{Tr(\int d^2r_1\ d^2r_2\ t(\vec{r_1})t(\vec{r_2})\rho(\vec{r_1},\vec{r_2}))} \tag{4}$$

We consider that the cavity is positioned at the focal point of a microscope objective, which transforms the emitted far field into the complex transverse shape of a propagative beam. In the first order approximation, Φ_H and Φ_V are real and positive, corresponding to the case where the transverse phase is constant in the propagative modes (plane wave approximation). Let k and e be:

$$k = \int d^2r\ t(\vec{r})\sqrt{\Phi_H(\vec{r})\Phi_V(\vec{r})} \tag{5}$$

$$e = \int d^2r\ t(\vec{r})\Phi_H^2(\vec{r}) = \int d^2r\ t(\vec{r})\Phi_V^2(\vec{r}) \tag{6}$$

The overlap factor K can be expressed as $K = k^2/e^2$ and the final expression of the detected photon density matrix in the case of non-maximal overlap of the two emission modes is:

$$\rho = \begin{pmatrix} \alpha & 0 & 0 & (d-ic_1)K \\ 0 & \frac{1}{2}-\alpha & c_2K & 0 \\ 0 & c_2K & \frac{1}{2}-\alpha & 0 \\ (d+ic_1)K & 0 & 0 & \alpha \end{pmatrix} \tag{7}$$

Note that only the coherence terms are modified, and are multiplied by the overlap factor K. When both modes do not overlap ($K = 0$), the mutual coherence is

erased and entanglement vanishes. On the contrary, maximally entangled states can only be obtained for $K = 1$. Following [14], Bell inequalities can be rewritten as $S = 2\sqrt{2}\,(\alpha + K * (d - c_2)) > 2$. Even in the case of a single dot emitting maximally entangled photons, a minimum overlap of $K > 2/\sqrt{2} - 1 = 41\%$ is required in order to violate Bell inequalities.

2. H1 cavity for maximally entangled photons

We consider the H1 cavity as potential candidate for the generation of entangled photon pairs since it sustains two energy degenerate dipole modes with a field maximum in the center of the cavity. This cavity offers both a low mode volume and theoretically high quality factors by fine tuning the inner holes [17].

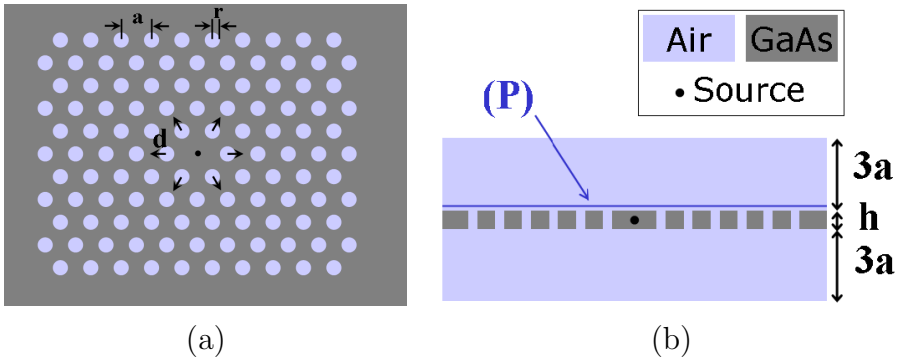

Figure 2. H1 photonic crystal cavity. The inner holes are shifted by the quantity d from 0 (standard H1 design) to 0.18a. The blue line is the plane where the field is registered at the end of the simulation for radiative pattern calculations.

Simulations of H1 cavities were performed with the 3D finite-difference time-domain (FDTD) method, using a freely available software package with subpixel smoothing for increased accuracy[18]. The simulated structure is depicted in figure 2. The H1 photonic crystal (figure 2(a)) has a lattice constant equal to a =270 nm and the holes have a radius of r_h =80 nm. The refractive index of the GaAs membrane is equal to n =3.46. Above and below the membrane, a free space volume is inserted, with a thickness of $3a$. The simulation volume is finally surrounded by Split Field Perfect Matched Layers (PML). A temporally short Gaussian dipole pulse (with a width of 10 optical oscillations) is launched in the center of the cavity (figure 2(b)) and used as a white light source. After extinction of the source, the electromagnetic field evolves freely over a time corresponding to approximately 300 optical cycles of the source, after which all low quality factor modes have radiated, thus leaving only the desired cavity mode in the simulation volume. In such conditions, the decay of the field amplitude at some fixed non-nodal point inside the cavity follows a simple exponential function of rate Γ_c. The emission wavelength is determined by measuring the optical oscillation frequency.

The collection efficiency is defined as the ratio between the incident power within a given emission cone normal to the membrane, over the total emitted power. At any given

time, the total emitted power is given by $P_{ref} = \Gamma' * W$ where W denotes the energy inside the cavity, and Γ' is the intensity decay rate ($\Gamma' = 2\Gamma_c$). Let U be the total energy in the simulated volume at time t. The energy outside the cavity (U_{out}) corresponds to the energy emitted by the cavity which has not yet reached the edge of the simulation volume, $U_{out} = \Gamma' * W * D/c$ with D being the radius of the simulated volume and c the speed of light. Thus $U = W * (1 + D/c)$. Since D is only a few micro-meters wide, $D/c << 1$, and the total emitted power can be written as $P_{ref} = 2\Gamma_c U$.

The emission mode of the cavity is estimated following reference [19] (mainly Eq. 23). This method relies on the complex value of the electromagnetic field on a plane (P) just above the membrane (see figure 2(b)) at some time (in our case the end of the simulation). The real part of the electromagnetic field is directly measured on (P), and the imaginary part is deduced from measurements of the real part of the electromagnetic field a quarter oscillation later (at the cavity's resonant frequency), taking into account the losses induced during this quarter of cycle. This allows us to extract the far field emission mode from the light-cone of the spatial Fourier transform of the field with a unique simulation run in real values, thus saving valuable calculation time. Emission patterns for a membrane thickness of $h = 0.26\mu m$ as a function of the hole displacement d are depicted in figure 3 and correspond qualitatively with the emission patterns calculated by Roemer *et al* [17] using a 3D Finite Element Maxwell Solver. For small hole displacements ($d \leq 0.10$), the emission diagram is almost spherical, whereas by increasing the hole displacement ($d \geq 0.14$), a pronounced, directional Gaussian-like, central peak appears.

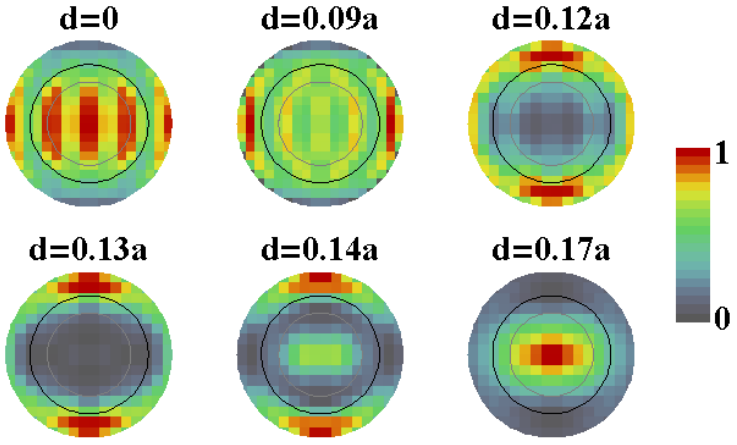

Figure 3. Emission patterns for various hole displacement d for a membrane thickness of h =0.26μm. Each pattern is normalized to its maximum value. The distance to the center is $sin(\theta)$ where θ is the normal angle to the membrane. The gray (resp. black) circle represents an objective of numerical aperture NA=0.5 (resp. NA=$sin(\pi/4) = 0.7$)

A systematic analysis of the maximal Purcell factor (F_p^{max}), collection efficiency (η), and mode overlap (K) has been performed by varying two parameters: the hole

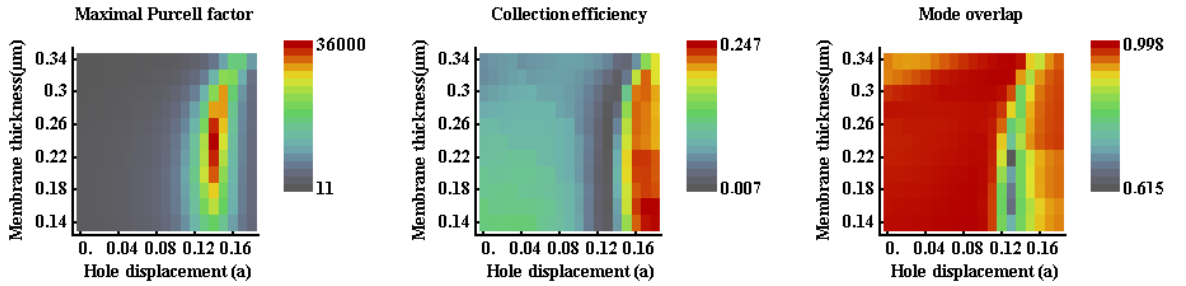

Figure 4. Maximal Purcell factor, collection efficiency, and mode overlap as a function of the hole displacement (d, in cristal units a) and membrane thickness (h, in μm).

displacement d and the membrane thickness h. Figure 4 summarizes the results where the mode overlap and collection efficiency are estimated for an objective with a numerical aperture of 0.5. By maximal Purcell factor, we mean the Purcell factor obtained for a resonant punctual monochromatic source placed at the maximum of the electrical field intensity. A more detailed view of the variation of these parameters as a function of the hole displacement is given in figure 5, in which the membrane thickness is fixed to $h = 0.26\mu m$ and three numerical apertures have been taken into account (0.2, 0.5 and 0.7). The wavelength λ_c of the cavity depends strongly on both parameters d and h. A good linear approximation is $\lambda_c = d \times 0.28\mu m + h \times 0.69 + 0.82\mu m$ with 4 nm of maximal deviation. A global homothetic transformation of the design, including the membrane thickness, should be latter applied to tune the cavity to the desired wavelength but is not taken into account here.

As we demonstrated earlier [14] a Purcell factor of 10 should be sufficient to restore entanglement in the emission cascade from single quantum dot. From this point of view alone, the whole domain of variation of the two parameters studied here satisfies this condition. However, spontaneous emission enhancement of the exciton rate is not sufficient to realize a deterministic efficient entangled photon source: efficient coupling of both photons to the cavity mode, high emission mode overlap and high collection efficiency are also needed. Let us first consider the coupling of both photons to the cavity mode. Exciton and biexciton lines are usually separated by about $2nm$. If the exciton is resonant with the cavity in order to obtain the highest spontaneous emission acceleration, the biexciton should preferably be also quasi-resonant with the cavity mode, in order to benefit from the redirection of the emission and to increase the collection efficiency of the biexcitonic photon. If we set a minimum Purcell factor for the quasi-resonant biexcitonic line to a value of about 5, this in turn limits the Purcell factor which can be reached for the excitonic line to a maximum value of about 110 for a cavity of modal volume $0.7(\lambda_c/n)^3$. This limitation excludes a large domain of parameters value around the hole shift of $d = 0.13$. Let us consider now the problem of emission mode overlap and collection efficiency. Since the highest collection efficiencies with a Gaussian-like emission pattern are reached for a membrane thickness of $h = 0.26\mu m$,

all further discussions are with this fixed value.

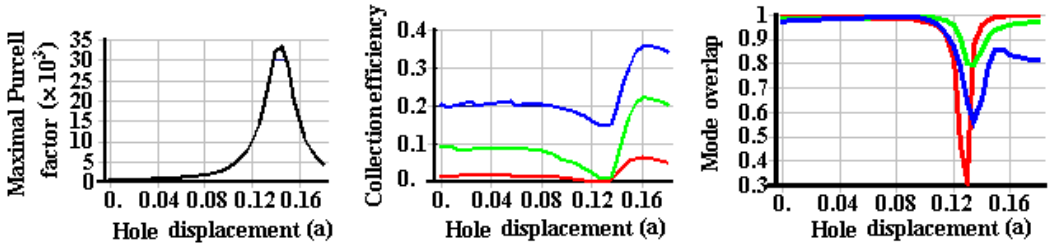

Figure 5. Maximal Purcell factor, collection efficiency, and mode overlap as a function of the hole displacement (d, in cristal units a) for a membrane thickness $h = 0.26\mu m$. The collection efficiency and the mode overlap are calculated for numerical apertures NA=0.2 (red curves), NA=0.5 (green curves) and NA=0.7 (blue curves).

At low hole displacement ($d \leq 0.09a$), high mode overlap can be obtained (in excess of 95%) but at the expense of a low collection efficiency (below 10% for standard microscope objectives (NA$\leq$ 0.5)) and does not exceed 22% for high numerical aperture objectives (NA=0.7) with a theoretical maximum of 50% since light is emitted upwards and downwards with the same intensity. The emission diagram (figure 3) for a hole displacement of d=0.1a clearly explains the situation. The mode is almost uniform in every direction giving rise to a high mode overlap, and the collection efficiency scales as the objective's numerical aperture. In the range $0.11a \leq d \leq 0.14a$ the mode overlap presents a distinct dip down to 57% for an objective with NA=0.7, and the collection efficiency drops to the same extent. In this region, the Purcell effect reaches its maximum (d=0.145a). The drop in the collection efficiency is correlated to the increase of the quality factor, corresponding to a better confinement of the light inside the photonic crystal slab and a reduction of vertical losses at the Γ point. For larger hole displacements ($d \geq 0.15a$) the collection efficiency increases sharply reaching 22% for a NA=0.5 (and $d = 0.16a$), corresponding to a 4-fold increase compared to a hole displacement of $d = 0.10a$. At the same time, the mode overlap increases up to 96% reaching almost the values obtained at low values of d. The mode profile (fig 3) is almost TE_{00} in the propagation direction perpendicular to the membrane. A numerical aperture of NA=0.2 increases the overlap up to almost 100% but at the expense of a low collection efficiency. On the other hand, a numerical aperture NA=0.7 increases the collection efficiency by a factor of 1.5 compared to a numerical aperture NA=0.5, but the mode overlap does not exceed 83% indicating that almost half of the energy is astigmatic. As a conclusion, a hole displacement of $d = 0.16a$ with an objective with numerical aperture of NA=0.5 and membrane thickness $h = 0.82\lambda_c/n$ seems to be the optimum in terms of collection efficiency (of the order of 22% with a maximal calculated value of 50%) and mode overlap (of the order of 96%).

3. Impact of the position of the dot in the cavity

Until now the quantum dot has been considered to be perfectly placed in the center of the cavity, implying that both polarizations undergo the same Purcell effect and that the cavity mode is equally fed for both polarizations. Deterministically aligning a photonic crystal around a single quantum dot so that the dot is positioned in the center of the cavity is technologically extremely challenging but mandatory. Several techniques are being developed [20, 21] although due to experimental uncertainties which are essentially due to the electronic beam lithography process, the mismatch of the quantum dot position with respect to the center of the H1 cavity can be up to 10 nm.

The position mismatch implies a breaking of the C_6 symmetry. The position of the dot will be identified by a direction X, as shown on figure 6(a), the Y direction being orthogonal to the X direction. The two polarization modes of the cavity remain unchanged. Therefore the sustained modes of the cavity will be described in the basis (X,Y) and no more in the (H,V) basis. Due to the mismatch with the cavity modes, the dipole will preferentially excite one of the modes (X or Y polarized) leading to an unbalance of the fraction β_i ($i \in [X, Y]$) of spontaneous emission in the cavity mode. Inevitably, this will in turn impact the entanglement visibility.

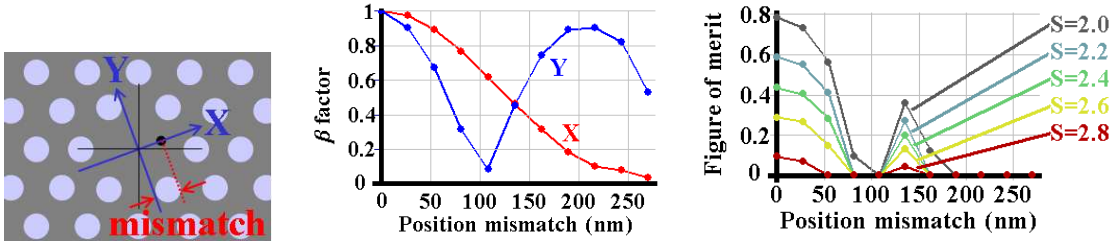

(a) (b) (c)

Figure 6. (a): Normalized β factor as a function of the position mismatch of the dot. The red (blue) curve corresponds to the X (Y) polarization. (b): Figure of merit ($r = T_1^{bulk}\delta\omega/(\hbar F_p^{max})$) as a function of the position mismatch for various values of the Bell test: S=2, S=2.2, S=2.4, S=2.6 and S=2.8.

Figure 6(b) depicts the normalized β_i factor as a function of the position mismatch along the X direction for both polarizations. The fraction of spontaneous emission for both polarizations (β_X and β_Y) at null mismatch; this permits us to normalize the β_i to 1 when the dot is centered, and use in our simulations the extrapolated amplitude of the corresponding mode divided by the amplitude of the whole field at the maximum of the excitation, in order to deduce the evolution of its β_i.

The effect of an asymmetric Purcell factor on the Bell's inequality is modeled in the annexe of this paper. If we want to reach some value S of the Bell test whereas the dot is misplaced, this puts a maximal limit to a figure of merit defined as the adimensional ratio $r = T_1^{bulk}\delta\omega/(\hbar F_p^{max})$ where T_1^{bulk} is the bulk lifetime of the dot,

$2\hbar\delta\omega$ the excitonic energy splitting and F_p^{max} the maximal Purcell effect of the cavity (at zero mismatch). Entanglement visibility increases when r tends to zero. This figure of merit only depends on the shortest lifetime that can be obtained in the dot-cavity system and on the quantum beat period between the two exciton states. Figure 6 (c) depicts the evolution of this figure of merit for different S values, calculated using the model introduced in the Annexe. For example, in the case of a centered dot with an excitonic bulk lifetime of 1 ns, an excitonic energy splitting of about $2\mu eV$, submitted to a maximal Purcell factor of 10 and not subjected to incoherent processes, the figure of merit $r = 0.3$ allows S to reach a value above 2.6. Conversely, the Bell's inequality is hardly violated ($S = 2$) if the same dot is about 70 nm away from the center of the cavity. For a more usual value of the excitonic splitting ($5\mu eV$), the maximal mismatch enabling for Bell's inequality violation drops to 10 nm.

4. Conclusion

In this paper we derived the Bell inequalities for a quantum dot in a photonic crystal cavity with non-overlapping polarization modes. By analyzing the emission pattern of modified H1 cavities, we demonstrate that it is possible to obtain both high collection efficiencies (of the order of 22%) and maximally overlapping modes while keeping high Purcell factors. Finally we estimate that the position of the quantum dot with respect to the cavity center has to be more accurate than 50 nm, in order to implement an efficient quantum dot source of polarization entangled photons from the biexciton cascade.

Acknowledgments

The authors would like to acknowledge L. Bernardi for technical support. This work has been founded by the NanoEPR project.

Annexe: effect of an assymetry in the Purcell effect

The asymmetric branching ratio induced by a polarisation dependant Purcell factor can be modelled as follows. Let the state of the system (dot and optical fields) be

$$|\Psi(t)\rangle = p_2(t)|2;\emptyset;\emptyset\rangle + \sum_{u=H,V}\int d\omega_2 p_u(\omega_2,t)|1_u;\overrightarrow{u},\omega_2;\emptyset\rangle + \sum_{u=H,V}\int d\omega_2 d\omega_1 p_{uu}(\omega_1,\omega_2,t)|0;\overrightarrow{u},\omega_2;\overrightarrow{u},\omega_1\rangle \quad (8)$$

where the first of the three entries within the ket refers to the quantum dot's level, the two other entries refer to the first and second emitted photons of polarisation $\overrightarrow{u}$ and pulsation ω_i (i=1, 2 respectively) (see figure 1. We distinguish here the emission rates γ_1 and γ_2 with respect to both polarizations H and V. We assume that incoherent processes are negligible, so that crossed terms combining horizontal and vertical orientations disappear.)

The expressions of the p_2, p_u and p_{uu} coefficients are determined using the Wigner-Weisskopf approximation. Considering the system at long times ($t >> 1/\gamma_1$ and γ_2) the terms $p_2(t)$ and $p_u(\omega_2, t)$ tend to zero, which gives a state that can be factorized into a radiative part $|\Psi_R\rangle$ and the fundamental source state $|0\rangle$. Considering no spectral filtering, the density matrix of the photon pair in the polarization basis is:

$$\rho = \int d\omega_1 d\omega_2 \langle \omega_2, \omega_1 || \Psi_R \rangle \langle \Psi_R || \omega_2, \omega_1 \rangle \tag{9}$$

$$= \sum_{u,v=H,V} |\overrightarrow{u}\,\overrightarrow{u}\rangle\langle\overrightarrow{v}\,\overrightarrow{v}| \int d\omega_2 d\omega_1 p_{uu}(\omega_1, \omega_2, \infty) p_{vv}(\omega_1, \omega_2, \infty)^* \tag{10}$$

$$= \frac{1}{2(1+2\delta F^2)} \begin{pmatrix} (\delta F+1)^3 & 0 & 0 & \frac{(1-\delta F^2)^2}{1-ig} \\ 0 & 0 & 0 & 0 \\ 0 & 0 & 0 & 0 \\ \frac{(1-\delta F^2)^2}{1+ig} & 0 & 0 & (\delta F-1)^3 \end{pmatrix} \tag{11}$$

where we defined the relative difference of Purcell factors $\delta F = (F_H - F_V)/(F_H + F_V)$ and the normalized splitting $g = 2\delta\omega/(\gamma_1^{bulk}(F_H + F_V))$. δF is approximated from the ration between the modal coupling factors as: $(\beta_H - \beta_V)/(\beta_H + \beta_V)$. In the same way as in [14], we deduce the expression S of the Bell test, from which we deduce data presented on figure 6(c).

References

[1] P. Shor, SIAM J. Computing **26**, 14841509 (1997)
[2] L.K. Grover, Phys. Rev. Lett. **79**, 325 - 328 (1997)
[3] D. Collins, N. Gisin and H. de Riedmatten, J. Mod. Opt **52**, 735-753 (2005)
[4] R. Ursin, T. Jennewein, M. Aspelmeyer, R. Kaltenbaek, M. Lindenthal and A. Zeilinger, Nature **430**, 849 (2004)
[5] O. Landry, J. A. W. van Houwelingen, A. Beveratos, H. Zbinden and N. Gisin, JOSA B **24**, 398-403 (2007)
[6] J.- .W Pan, D Bouwmeester and H Weinfurter Phys. Rev. Lett. **80**, 3891 (1998)
[7] M. Halder, A. Beveratos, N. Gisin, V. Scarani, C. Simon and H. Zbinden" Nature Phys **3** 3, 692 (2007)
[8] X. Li, P. L. Voss, J. E. Sharping and P. Kumar Phys. Rev. Lett. **94**, 053601 (2005)
[9] J. Fulconis, O. Alibart, J. L. O'Brien, W. J. Wadsworth and J. G. Rarity Phys. Rev. Lett. **99**, 120501 (2007)
[10] V. Scarani, H. de Riedmatten, I. Marcikic, H. Zbinden and N. Gisin, Eur. Phys. J. D. **32**, 129 (2005)
[11] O. Benson, C. Santori, M. Pelton and Y. Yamamoto, Phys. Rev. Lett. **84**, 2513 (2000)
[12] N. Akopian, N. H. Lindner, E. Poem, Y. Berlatzky, J. Avron, D. Gershoni, B. D. Gerardot and P. M. Petroff, Phys. Rev. Lett. **96**, 130501 (2006)
[13] R.M. Stevenson, R.J. Young, P. Atkinson, K. Cooper, D.A. Ritchie and A.J. Shields, Nature (London) **409**, 179 (2006)
[14] M. Larqu, A. Beveratos and I. Robert-Philip Phys. Rev. A **77**, 042118 (2008)
[15] W.L. Barnes, G. Björk, J.M. Gérard, P. Jonsson, J.A.E. Wasey, P.T. Worthing and V. Zwiller, Eur. Phys. J. D **18**, 197 (2002)
[16] L. Balet, M. Francardi and A. Gerardino, N. Chauvin, B. Alloing, C. Zinoni, C. Monat, L. H. Li, N. Le Thomas, R. Houdr, and A. Fiore Appl. Phys. Lett. **91**, 123115 (2007)
[17] F. Roemer and B. Witzigmann, JOSA B **25**, 31 (2008)

[18] A. Farjadpour, D. Roundy, A. Rodriguez, M. Ibanescu, P. Bermel, J. D. Joannopoulos, S. G. Johnson and G. Burr, Optics Letters **31**, 2972 (2006)
[19] J. Vuckovic, M. Loncar, H. Mabuchi and A. Sherer, IEEE Journ. Quant. Elect. **38**, 850 (2002)
[20] A. Badolato, K. Hennessy, M. Atature, J. Dreiser, E. Hu, P. M. Petroff, A. Imamoglu, Science **308**, 1158 (2005)
[21] N. Gogneau, L. Le Gratiet, E. Cambril, G. Beaudoin, G. Patriarche, A. Beveratos, R. Hostein, I. Robert-Philip, J.Y. Marzin, I. Sagnes Journal of Crystal Growth **310**, 3413-3415 (2008)